Planar selective Leidenfrost propulsion without physically structured substrates or walls

Linzi E. Dodd (iD), Prashant Agrawal (iD), Nicasio R. Geraldi (iD), Ben B. Xu (iD), Gary G. Wells (iD), James Martin (iD), Michael I. Newton (iD), Glen McHale (iD), and David Wood (iD)

View Online   **Export Citation**   **CrossMark**

ARTICLES YOU MAY BE INTERESTED IN

Planar selective Leidenfrost propulsion without physically structured substrates or walls

View Online · Export Citation · CrossMark

Linzi E. Dodd,[1,a] Prashant Agrawal,[1] Nicasio R. Geraldi,[2] Ben B. Xu,[1] Gary G. Wells,[1] James Martin,[1] Michael I. Newton,[2] Glen McHale,[1] and David Wood[1]

AFFILIATIONS

[1]Smart Materials and Surfaces Laboratory, Faculty of Engineering and Environment, Northumbria University, Newcastle Upon Tyne NE1 8ST, United Kingdom
[2]School of Science and Technology, Nottingham Trent University, Nottingham NG11 8NS, United Kingdom

[a]Author to whom correspondence should be addressed: linzi.dodd@northumbria.ac.uk

ABSTRACT

The Leidenfrost effect allows droplets to be transported on a virtually frictionless layer of vapor above a superheated substrate. The substrates are normally topographically structured using subtractive techniques to produce saw-tooth, herringbone, and other patterns and bulk heated, leading to significant challenges in energy consumption and controlled operation. Here, we propose a planar lithographic approach to levitate and propel droplets using temperature profiles, which can be spatially patterned and controlled in time. We show that micro-patterned electrodes can be heated and provide control of the pressure profile and the vapor flow. Using these almost featureless planar substrates, we achieve self-directed motion of droplets, with velocities of approximately 30 mms^{-1}, without topographically structuring the substrate or introducing physical walls. Our approach has the potential to be integrated into applications, such as digital microfluidics, where frictionless and contactless droplet transport may be advantageous.

The Leidenfrost effect is a case of thin film boiling where, when a droplet contacts a surface that is significantly hotter than the liquid's boiling point, the droplet levitates on a cushion of its own vapor.[1] The vapor layer thermally insulates the drop from the hot surface, increasing the droplet's lifetime, and provides lubrication, which results in increased mobility. Recently, there has been significant interest in this effect to create an effectively perfect superhydrophobic surface, reduce friction, and propel droplets (or a solid block of dry ice undergoing sublimation).[2–4] To produce propulsion, asymmetries are introduced into the flow of the exiting vapor, either by structuring the substrate asymmetrically[5–7] or by an asymmetric mass distribution.[8,9] The most common explanation of the propulsion mechanism is that asymmetric vapor flow produces a viscous drag on the levitating component and causes the droplet to translate or rotate in a preferential designed direction.[10,11] Propulsion can be obtained using different structures employing local asymmetries like ratchets[12–15] or global asymmetrical shapes like herringbones,[6,16,17] which are produced using, e.g., subtractive manufacturing techniques. Inducing levitation and controlling drop motion on these surfaces are energy intensive as the entire substrate has to be bulk heated.

In this work, we propose selectively heated substrates to propel and control the motion of droplets using photolithographic patterning of metal films in an asymmetric pattern. The substrates are obtained by planar deposition of electrodes in an asymmetric pattern. By selectively heating the substrate via Joule heating of the electrodes, the input energy to induce levitation is reduced significantly,[18] while patterns of thermal gradients on the substrate are used to rectify the vapor flow for propulsion. We also employ concepts of shaped liquid-vapor interfaces using thermal gradients[19] to control the position of these highly mobile droplets using negative feedback control. We, therefore, introduce a highly flexible virtual method to produce the equivalent propulsion and control to ratchet and herringbone structures and physical walls without the need to physically shape the substrate or introduce walls.

As an example of a herringbone-inspired structure, we designed resistor line patterns using serpentine electrode designs 40 μm wide, repeated four times, with a 40 μm gap between each line (Fig. 1 inset left). This array of 4 serpentine lines acts as a lithographic "heater," which is repeated with a gap of 1.0 mm, as shown in Fig. 1. The electrode heaters model the pillars (here, we refer to these as "virtual
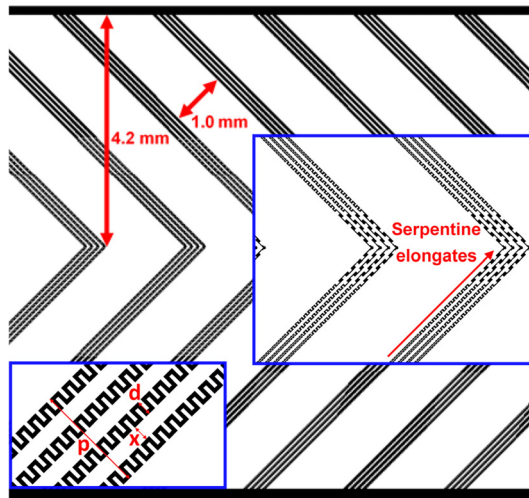
FIG. 1. Self-centering herringbone design, showing (inset right) elongation of the serpentine pattern when approaching the center of the design and (inset lower left) the standard serpentine design, with line widths of 10 μm, pattern widths of d = 40 μm, and a gap between each serpentine line of x = 40 μm, which results in a lithographic virtual pillar width of p = 280 μm and a virtual trough of 1.0 mm.

pillars") and the gaps between these heaters represent the trough region (here, we refer to these as "virtual troughs") in a subtractive machined herringbone feature.[6]

An additional development of the herringbone structure was the addition of elongated (gradient) serpentine patterns to change the current density at different positions relative to the center of the herringbone structure, in order to achieve a self-centering design for droplet motion as shown in Fig. 1. This results in a temperature distribution with a higher temperature at the edges of the design relative to that in the central region. In the plain herringbone-inspired pattern, with a uniform serpentine design, such a temperature variation will not exist between the sides and the center of the design.

We used a bi-layer lift-off process to produce the metallic pattern on the borosilicate glass substrates. PMGI SF9 is spun onto the substrate at 500 rpm for tens and then at 6000 rpm for 50 s using a Laurell spinner, resulting in a layer approximately 500 nm thick. This layer is then baked at 200 °C for 5 min. Microposit SPR-350 photoresist is spun on top of this baked layer at 700 rpm for tens and then 3700 rpm for 50s using a Laurell spinner and baked at 110 °C for 3 min. A dark field chromium mask is then used in an EVG 620 mask aligner to expose regions of the substrate to UV light for 4 s. The substrate is then developed for 2 min using an MF-319 developer, ensuring undercutting of the SPR-350 by the SF9. 10 nm of titanium, 20 nm of platinum, and 100 nm of gold are then deposited in the same e-beam evaporation process. The excess metal is removed by removing the photoresist below the metal, using a Microposit 1165 stripper, leaving the required resistor patterns.

Each wafer contains the desired design and contact pads to ensure an electrical connection. In order to ensure experimental repeatability, a custom rig is designed for the experiments, with an mbed-controlled Peltier cooler with cooling pipes and fan on the underside to maintain a uniform temperature within the stage. Spring loaded electrical contacts are used to pass a current through the

patterned electrodes. A USB optical microscope is used to observe the drop motion, and a FLIR A40 thermal camera is used to observe the temperature profile of the substrate. An appropriate power is identified for levitation and the array is left for 1 minute for the temperature to equalize before depositing a 20 μl droplet of propan-2-ol (IPA) to observe propulsion.

Figure 2 show the motion of IPA droplets on the herringbone-inspired patterned surfaces with a uniform [Fig. 2(a)] and gradient [Fig. 2(b)] serpentine spacing. In Fig. 2(a), the droplets travel "against the arrows" in the pattern, which is like the motion of droplets on the features of a herringbone surface.[6] It was determined that varying the "trough" width impacted the ability of the substrate to propel the droplet. Both 0.6 mm and 0.8 mm wide troughs caused droplet propulsion, as seen in the supplementary videos. On the herringbone design, a drop deposited near the center does not remain in the center due to the absence of any restoring force or any physical barriers inhibiting the outward motion. The self-centering design [Fig. 2(b)] provides this restoring force due to a negative temperature gradient from the sides toward the center. This negative temperature gradient is caused by the
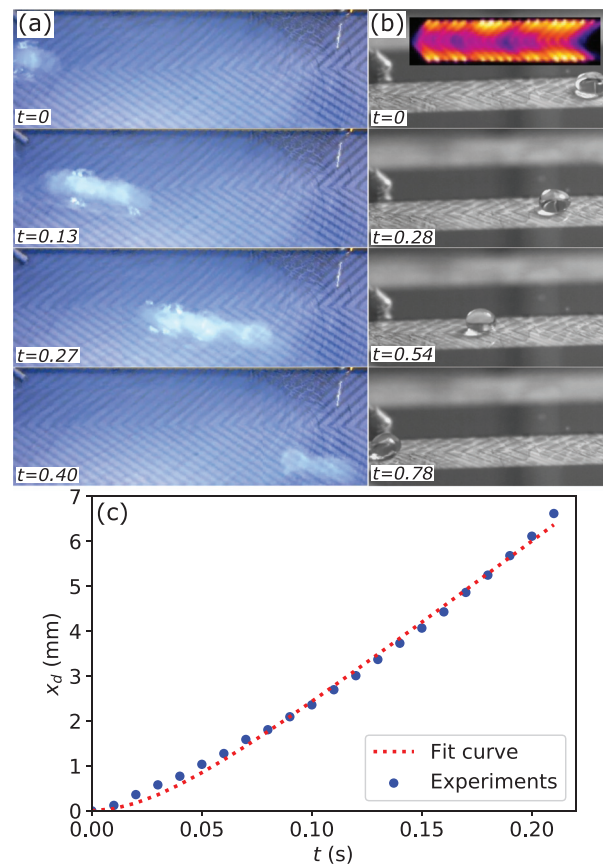
FIG. 2. (a) Droplet motion on a plain herringbone-inspired design (with uniform serpentine spacing) with a 0.6 mm wide trough; (b) droplet motion on a self-centering design (with a gradient serpentine spacing between the center and the sides) with a 1.0 mm width trough, and the inset shows a thermal image of the surface; (c) typical droplet motion tracking on a self-centering design with Eq. (3) fitted to the experimental data.

current density gradient due to the elongation of the serpentine shape. The higher temperature regions (near the substrate edges) work as a virtual barrier deflecting the droplets back to the center. Furthermore, this inverts the direction of travel, relative to the non-centering design. In the self-centering design, the droplets travel "with the arrows" due to the thermal gradient. It was also found that a trough width for the propulsion of centered droplets was 1.0 mm, as seen in Fig. 2. This gap reflects the dimensions of herringbone propulsion described by Soto et al.[6]

Figure 2(c) shows a typical displacement curve for a droplet on these planar surfaces, where droplets have an initial velocity of 16 mms^{-1} and an average velocity of 31 mms^{-1} over the first 0.2 s of motion. The droplets do not reach a terminal velocity and would, therefore, continue to accelerate on a larger sample. Assuming a viscous drag driven constant propulsion force (F_p) and negligible inertial resistance to the motion from the surface pattern, a droplet's motion can be characterized from the following equation of motion:

$$m\dot{v}_d = F_p - c_v v_d, \qquad (1)$$

where F_p is the propulsion force, m is the mass of the droplet, v_d is the droplet velocity, and c_v is the coefficient of viscous resistance. The solution to Eq. (1) is

$$v_d = v_t(1 - e^{-t/\tau}), \qquad (2)$$

where v_t is the terminal velocity and τ is the relaxation time, which is a measure of the drop's acceleration. The droplet's position (x_d) is given by

$$x_d = v_t(t + \tau e^{-t/\tau}). \qquad (3)$$

Equation (3) agrees well with the experimental data in Fig. 2(c). As a result, we obtain the terminal of $v_t = 36.4$ mms^{-1} and the relaxation time $\tau = 0.04$ s.

For the substrate designs with gradient serpentine patterns, multiple designs with different elongation dimensions were tested. It was observed that designs where the central serpentine resistors were elongated by 10% between the edge and the center provided the optimal propulsion performance. A higher elongation resulted in arrays where the central region could not heat sufficiently to support levitation, without compromising outer resistor damage with excessive heat. A smaller elongation did not generate enough of a temperature difference between the edge and the center of the substrate to achieve self-centering.

To qualitatively explain the propulsion observed in our experiments, we develop a 2D model to observe the flow field over a substrate with a sinusoidal temperature distribution: $T_s = T_0 + \alpha \cos(2k\pi x/L)$, where $k \geq 3$, as depicted in Figs. 3(a) and 3(b). This sinusoidal temperature profile is an approximation to the temperature profile on the substrates used in the experiments. Assuming that the heat transfer occurs through conduction in the vapor layer and is used for phase change of the liquid, the evaporative velocity w_0 is obtained as[15]

$$w_0 = \frac{\lambda(T_s - T_b)}{\rho_v L_v h}, \qquad (4)$$

where h is the vapor layer thickness, λ is the thermal conductivity of the vapor layer, T_b is the boiling point of the liquid, ρ_v is the density of
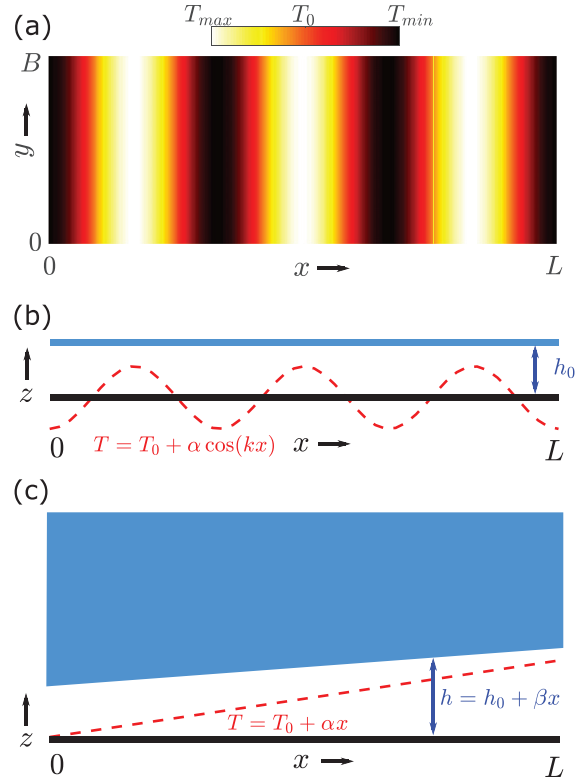
FIG. 3. Analytical model setup depiction: (a) 2D model: sinusoidal temperature distribution in x on a substrate with length L and breadth B; (b) 2D model: depiction of the xz view with a constant vapor layer thickness; (c) 1D model: depiction of the varying vapor layer thickness on a substrate with a linear temperature variation.

the vapor layer, and L_v is the latent heat of vaporization of the liquid. Invoking the lubrication approximation, the velocity in the x direction (u) and the velocity in the y direction (v) can be written as[15]

$$u = -\frac{1}{2\mu_v}\frac{\partial p}{\partial x}z(z - h), \qquad (5)$$

$$v = -\frac{1}{2\mu_v}\frac{\partial p}{\partial y}z(z - h), \qquad (6)$$

where p is the pressure in the vapor layer and μ_v is the dynamic viscosity of the vapor. Using Eqs. (5) and (6) in the continuity equation ($\nabla \cdot \mathbf{u} = 0$) and integrating it from $z = 0$ to $z = h$, with the boundary conditions: at $z = 0$, $w = 0$ and at $z = h$, $w = -w_0$, we obtain

$$\nabla^2 p = c_0 + c_1 \cos\left(\frac{2k\pi x}{L}\right), \qquad (7)$$

where $c_0 = -12\mu_v\lambda(T_0 - T_b)/(\rho_v L_v h^4)$ and $c_1 = -12\mu_v\lambda\alpha/(\rho_v L_v h^4)$ are constants. The solution to Eq. (7) is of the form[20]

$$p(x, y) = \Sigma_{m=0}^{\infty}\Sigma_{n=0}^{\infty} P_{m,n}\sin\left(\frac{m\pi x}{L}\right)\sin\left(\frac{n\pi y}{B}\right), \qquad (8)$$

where $P_{m,n}$ is a constant obtained as (additional details on the derivation are provided in the supplementary material)

$$P_{m,n} = \left[\frac{4c_0}{mn\pi^2} + \frac{4c_1 m}{(m^2 - 4k^2)n\pi^2} \right] \frac{\left[1 - (-1)^m\right]\left[1 - (-1)^n\right]}{(m\pi/L)^2 + (n\pi/B)^2}. \quad (9)$$

In the pressure field obtained from Eq. (8), the terms with c_0 are the zeroth order solution [Fig. 4(a)], which corresponds to the pressure field on a uniformly heated substrate. The coefficient terms with c_1 constitute the first order solution, which corresponds to the perturbations due to the temperature field's spatial variation [Fig. 4(a)]. Therefore, the first order velocity field contains information about the vapor flow due to the thermal gradients. Figure 4(b) shows that the vapor flow diverges from regions of higher temperature and converges to regions of lower temperature. In this model, the flow is symmetric about x and y, and therefore, the net propulsion force from this flow in these directions is zero. However, in a V-shape arrangement, as used in the experiments (Fig. 1), this vapor rectification causes a net flow in the x direction, propelling droplets deposited near the centers against the arrows, similar to that observed in herringbone-like structures obtained through subtractive manufacturing techniques.[6] Also, as the flow along y diverges from the center of this V-shaped geometry, the drop is unstable and minor perturbations deflect the drop from the center, as observed in Fig. 2(a). It is important to note here that

this theoretical model is a simplified system compared to the complexities of drop motion in experiments. Approximations such as a sinusoidal temperature field assumption in x, a symmetric temperature field in y, a flat liquid-vapor interface, and a rectangular interface cross section (as opposed to circular) affect an accurate estimation of the scale of forces acting on the drop. However, the model qualitatively provides information about the direction of vapor flow that drives the motion.

A similar vapor rectification between the electrode patterned regions also occurs in the self-centering design. However, the additional thermal gradient along the electrodes shapes the liquid-vapor interface and results in a pressure gradient between the center and the sides. The direction of this pressure gradient generated force can be adjudged by considering a simplified 1D model with a liquid levitating on a substrate with a linear temperature distribution: $T_s = T_0 + \alpha x$, as depicted in Fig. 3(c). We use this simplified approach to obtain qualitative estimates of the direction of propulsion as opposed to using complete numerical solutions of the liquid-vapor interface profile as used by Sobac et al.[19]

Invoking the lubrication approximation, the flow in the x-direction can be written by Eq. (5). The shear force (per unit width) on the liquid-vapor interface (F_s) can be written as

$$F_s = \mu_v \int_{-L}^{L} \left. \frac{\partial u}{\partial z} \right|_{z=h} dx. \quad (10)$$

The temperature distribution on the substrate creates a difference in pressure between the hot and cold ends, which shapes the liquid-vapor interface. Considering a first-order approximation, we assume a linearly varying vapor layer thickness: $h = h_0 + \beta x$, as shown in Fig. 3(c). The dynamics of motion induced due to this shaped-liquid interface is similar to the propulsion of uneven solids.[8,14] With the boundary condition of $p = 0$ at $x = 0$ and $x = L$, using Eq. (5) in Eq. (10), the shear force can be written as $F_s = \frac{\beta}{2} \int_{-L}^{L} p \, dx$. The total propulsion force (F_p) is given by the sum of the shear force (F_s) and the normal force ($F_n = -\int_{-L}^{L} p \, dx \sin \beta$) on the liquid-vapor interface in the x direction[8]

$$F_p \approx -\frac{\beta}{2} \int_{-L}^{L} p \, dx. \quad (11)$$

The normal force due to the pressure field will balance the weight of the levitating liquid (mg)

$$\int_{-L}^{L} p \, dx \cos \beta = mg. \quad (12)$$

Also, the net torque on the levitating liquid will be zero

$$\int_{-L}^{L} px \, dx \cos \beta = \frac{mgH \sin \beta}{2}. \quad (13)$$

The above two equations provide the pressure field p and β (derivation details in the supplementary material). The normal pressure due to the deformed liquid-vapor interface contributes to the propulsion,[8] where the direction of motion is from the region of higher temperatures to lower temperatures, in agreement with the numerical predictions of Sobac et al.[19] The self-centering designs in our experiments rely on this force to center droplets. As a drop traverses off-center, the negative temperature gradient toward the center shapes the

FIG. 4. (a) Normalized second order pressure profile (p_2); the inset shows the normalized first order pressure profile (p_1); (b) normalized second order velocity field profile in x (u_2) at $y = B/2$; the inset shows the normalized first order velocity field profile in x (u_1) at $y = B/2$; the arrows depict the net direction of the u_2 flow field, which converges to the low temperature regions.

liquid-vapor interface, which produces a force toward the center. Once the droplet reaches the center, the vapor rectification between the electrodes propels it in the x direction.

In this work, we have used planar surfaces to propel droplets. We have used lithographic techniques to pattern micro-heater arrays on a substrate, which provide selective heating to sustain levitation. The asymmetric macro-pattern of these arrays has been tailored to provide a temperature differential, which propels and, using a negative feedback control, self-centers droplets on the substrate, similar to substrates using physical features produced by subtractive machining. Our concepts of motion induced as a result of a thermal gradient using selective programmable heating can be used to develop energy efficient devices for droplet motion control in microfluidic systems, which can be fabricated more readily using standard lithographic techniques.

See the supplementary material for additional information on the analytical model, as well as a video of propulsion in a non-centered design (Fig. S1) and a centered design (Fig. S2).

DATA AVAILABILITY

The data that support the findings of this study are available within the article and its supplementary material.

REFERENCES

[1]J. G. Leidenfrost, "On the fixation of water in diverse fire," Int. J. Heat Mass Transfer **9**, 1153–1166 (1966).

[2]D. Quéré, "Leidenfrost dynamics," Annu. Rev. Fluid Mech. **45**, 197–215 (2013).

[3]G. Dupeux, P. Bourrianne, Q. Magdelaine, C. Clanet, and D. Quéré, "Propulsion on a superhydrophobic ratchet," Sci. Rep. **4**, 5280 (2015).

[4]L. Zhong and Z. Guo, "Effect of surface topography and wettability on the Leidenfrost effect," Nanoscale **9**, 6219–6236 (2017).

[5]G. Lagubeau, M. L. Merrer, C. Clanet, and D. Quéré, "Leidenfrost on a ratchet," Nat. Phys. **7**, 395–398 (2011).

[6]D. Soto, G. Lagubeau, C. Clanet, and D. Quéré, "Surfing on a herringbone," Phys. Rev. Fluids **1**, 013902 (2016).

[7]L. E. Dodd, P. Agrawal, M. T. Parnell, N. R. Geraldi, B. B. Xu, G. G. Wells, S. Stuart-Cole, M. I. Newton, G. McHale, and D. Wood, "Low-friction self-centering droplet propulsion and transport using a Leidenfrost herringbone-ratchet structure," Phys. Rev. Appl. **11**, 034063 (2019).

[8]G. Dupeux, T. Baier, V. Bacot, S. Hardt, C. Clanet, and D. Quéré, "Self-propelling uneven Leidenfrost solids," Phys. Fluids **25**, 051704–051707 (2013).

[9]A. Bouillant, T. Mouterde, P. Bourrianne, A. Lagarde, C. Clanet, and D. Quéré, "Leidenfrost wheels," Nat. Phys. **14**, 1188 (2018).

[10]H. Linke, B. J. Alemán, L. D. Melling, M. J. Taormina, M. J. Francis, C. C. Dow-Hygelund, V. Narayanan, R. P. Taylor, and A. Stout, "Self-propelled Leidenfrost droplets," Phys. Rev. Lett. **96**, 2–5 (2006).

[11]T. Baier, G. Dupeux, S. Herbert, S. Hardt, and D. Quéré, "Propulsion mechanisms for Leidenfrost solids on ratchets," Phys. Rev. E **87**, 3–6 (2013).

[12]J. M. Arter, D. J. Cleaver, K. Takashina, and A. T. Rhead, "Self-propelling Leidenfrost droplets on a variable topography surface," Appl. Phys. Lett. **113**, 243704 (2018).

[13]R. L. Agapov, J. B. Boreyko, D. P. Briggs, B. R. Srijanto, S. T. Retterer, C. P. Collier, and N. V. Lavrik, "Asymmetric wettability of nanostructures directs Leidenfrost droplets," ACS Nano **8**, 860–867 (2014).

[14]H. Xu, A. Thissandier, R. Zhao, P. Tao, C. Song, J. Wu, W. Shang, and T. Deng, "Self-propelled rotation of paper-based Leidenfrost rotor," Appl. Phys. Lett. **114**, 113703 (2019).

[15]G. G. Wells, R. Ledesma-Aguilar, G. McHale, and K. Sefiane, "A sublimation heat engine," Nat. Commun. **6**, 6390 (2015).

[16]P. Agrawal, G. G. Wells, R. Ledesma-Aguilar, G. McHale, A. Buchoux, A. Stokes, and K. Sefiane, "Leidenfrost heat engine: Sustained rotation of levitating rotors on turbine-inspired substrates," Appl. Energy **240**, 399 (2019).

[17]D. Soto, H. De Maleprade, C. Clanet, and D. Quéré, "Air-levitated platelets: From take off to motion," J. Fluid Mech. **814**, 535–546 (2017).

[18]L. E. Dodd, D. Wood, N. R. Geraldi, G. G. Wells, G. McHale, B. B. Xu, S. Stuart-Cole, J. Martin, and M. I. Newton, "Low friction droplet transportation on a substrate with a selective Leidenfrost effect," ACS Appl. Mater. Interfaces **8**, 22658–22663 (2016).

[19]B. Sobac, A. Rednikov, S. Dorbolo, and P. Colinet, "Self-propelled Leidenfrost drops on a thermal gradient: A theoretical study," Phys. Fluids **29**, 082101 (2017).

[20]M. Greenberg, *Advanced Engineering Mathematics* (Prentice Hall, New Jersey, 1998).